

Nawfal A. Noori
Kadhim A. Aadim

Department of Physics,
College of Science,
University of Baghdad,
Baghdad, IRAQ



Spectroscopic Diagnostics of Cu:Al Plasma Produced by DC Magnetron Discharge at Different Working Conditions

In this study, a spectroscopic study on Cu:Al co-sputtering was investigated in detail. The study includes the effect of varying vacuum pressures and applied voltages on plasma parameters to optimize these operational parameters that lead to enhanced sputtering efficiency. An important finding is the optimal Ar pressure at 0.3 mbar, and the electrical discharge was enhanced directly with the applied voltage. The highest emission intensity emitted from the sputtered species, electron temperature (T_e), and electron number density (n_e) occurred at the same 0.3 vacuum pressure. They demonstrated a technique of observation of the plasma in the Cu: Al co-spraying system and their effect on the sputtering process.

Keywords: Plasma parameters; Optical Emission Spectroscopy; Sputtering; Optimization
Received: 07 June 2024; Revised: 30 July 2024; Accepted: 06 August 2024

1. Introduction

Among the various spectroscopic methods, optical emission spectroscopy (OES) is the most common for analyzing plasma properties [1]. OES includes analyzing the electromagnetic radiation emitted by excited atoms and ions inside the plasma [2,3], which enables the understanding of plasma properties related to the sputtering process and thin film deposition [4].

The study of plasma properties through spectroscopic analysis is essential in sputtering systems for nanoparticle generation [5] and thin film deposition because the plasma components and their kinetic properties are responsible for the sputtering process [6,7]. Plasma properties play an essential role in the sputtering process because they are directly related to the dynamics of different species [8], which affect the properties of the deposited thin films [9].

The working parameters of the direct current sputtering system affect the energy of the ions bombarding the target materials, cause significant differences in plasma properties, and significantly affect the formation and properties of the deposited film [10,11]. Through spectroscopic study, the influence of operating conditions such as vacuum pressure and applied voltage on the plasma behavior can be distinguished, which is related to the elemental distribution, species concentration, energy distribution [12], and ionization degree [13,14]. These investigations lead to improved deposition of thin films with the desired properties for specific applications, from microelectronics to advanced coatings [15].

The co-sputtering process, which involves the simultaneous deposition of two materials, increases the complexity of plasma dynamics [16,17]. The spectroscopic investigation of plasma emission determines the critical interactions within the plasma and the proportions of materials sputtered from the

two electrodes in the co-sputtering system under different deposition conditions [18]. Emission spectroscopy provides information about the composition of plasma at different deposition parameters, which determines the probability of interaction between atoms and ions using information about their energies and number densities [19,20].

This work aims to study the plasma properties of a direct current co-sputtering system for copper and aluminum and to determine their variations under different Argon gas pressures and applied voltages to optimize the sputtering process. The study of plasma properties involves the variation in electron number density and temperature with vacuum pressure and applied voltage using optical emission spectroscopy (OES). In this work, the effect of the operational parameters of the co-sputtering system on the plasma parameters and the intensity of the emitted spectral lines of the two sputtered metals was studied, and their relationship with the sputtering efficiency of both metals and the deposition of thin films was investigated.

2. Experimental Setup

The co-sputtering system contains a cylindrical glass chamber with dimensions of 40 cm in diameter and 40 cm in height, as schematically shown in Fig. (1). The chamber was evacuated using Edwards rotary and diffusion vacuum pumps to achieve a base pressure of 1.0×10^{-6} mbar to ensure that the chamber was free of contaminants. Then, the introduction of argon (Ar) gas was controlled using a needle valve while the vacuum system was still running to reach the required vacuum level for the study. The distance between each cathode and the anode was fixed at 8 cm throughout the experiments. Two targets of Al and Cu, each with a diameter of 5 cm, were used, equipped with magnetrons behind the targets. These two targets were directed downward at 45° toward the

center of the anode. The working pressure at different operating levels (0.05, 0.1, 0.2, 0.3, and 0.4 mbar, and the voltages applied to both targets were varied at 400, 600, 800, 1000, and 1200 V to explore the effect of changing the spray pressure and applied voltage on the plasma properties. A Thorlabs CCS 100/M spectrometer with an optical fiber directed to the plasma glow point between the two targets was used to analyze the emission spectra of the plasma plume under different operating conditions. This spectrometer operates within the wavelength range of 200-1000 nm.

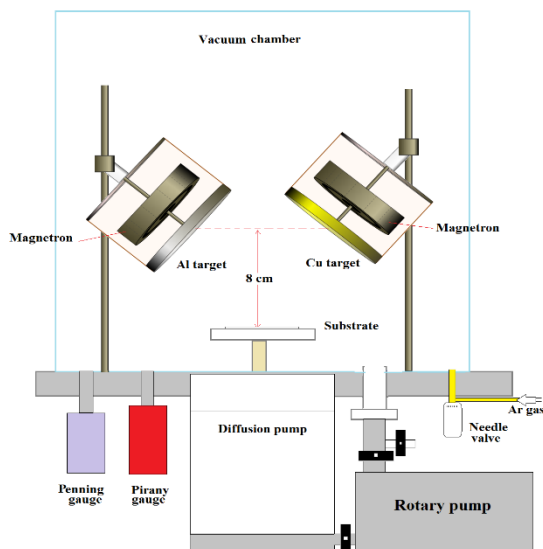


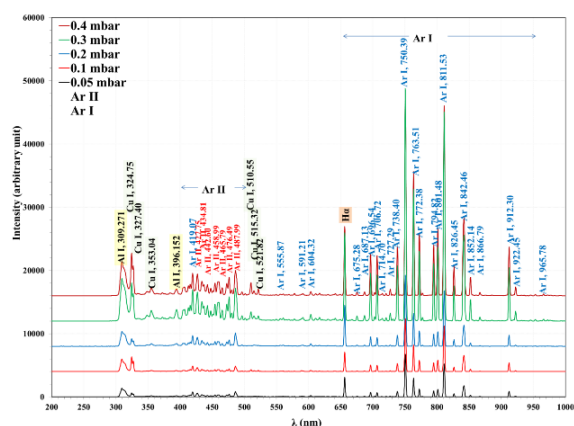
Fig (1) A scheme of the co-sputtering system in the laboratory of plasma physics at the Department of Physic, College of Science, University of Baghdad

3. Results and Discussions

Figure (2) depicts the spectroscopic patterns of plasma emission from the co-sputtering process of copper and aluminum targets using 1200V and varying operational gas pressures, ranging from 0.05 to 0.4 mbar. The observed emission lines were matched with the reference lines of electronic transitions in the atomic and ionic form of aluminum (Al), copper (Cu), and argon (Ar) from the database of the National Institute of Standards and Technology (NIST) [21]. The difference in intensity for different lines exhibited by each emission pattern is attributed to the variations in transition probabilities and the statistical weights associated with each transition. It also varies according to temperature according to Boltzmann distribution [22].

The emission intensity corresponding to atomic species is more evident than ionic ones, indicating the induced plasma's relatively low ionization levels [23]. The higher intensity corresponding to argon (Ar) lines than the others is attributed to the higher argon concentration compared to the relatively minor presence of sputtered metal atoms in the gas phase. Additionally, increased emission line intensity was observed with increasing working pressure up to 0.3 mbar. Meanwhile, intensity decreased as the pressure

was further increased to 0.4 mbar. At lower pressures, a limited number of inelastic collisions occur between the highly energetic electrons and the heavy species of atoms and ions, resulting in a lower emission intensity due to the low number of excitation collisions. As the working pressure is increased to an intermediate range of 0.3 mbar, a notable enhancement in emission line intensity was observed, which can be attributed to increasing cross-sectional area for electron-atom excitation collisions [24,25]. An increase in the excitation probability causes more photons to be emitted, so an increase in the emission intensity is observed [26]. However, line intensity was reduced with the operational pressure of 0.4 mbar. Increasing pressure to a higher level intensifies the collisional interactions between electrons and the background gas molecules. The heightened collision causes them to lose energy before reaching the threshold required for excitation or ionization collisions. Consequently, the emission intensity experiences a decline, effectively reflecting the competitive nature between excitation collisions and other collisions [27].



species to populate higher energy states, which cause higher emission line intensities.

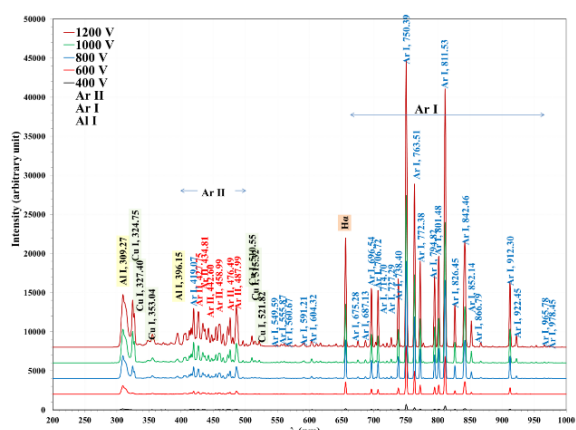


Fig. (3) Emitted spectra during co-sputtering of Cu:Al at 0.3 mbar vacuum pressures in Ar using different applied voltages

Additionally, it's important to note that the intensities of different emission lines increase in various ratios. According to the Boltzmann distribution, higher temperatures lead to a more population process into higher energy states. Thus, emission lines associated with transitions from higher energy levels have more intensity [28].

Figure (4) illustrates the variations in emitted line intensity of the sputtered metal atoms of Al I, 309.27, and Cu I, 324.75 intensity with working pressure and the applied voltage. The line intensity corresponding to the sputtered atoms indicates the sputtering efficiency. The higher intensity of these emission lines appeared at a vacuum pressure of 0.3 mbar, which indicates that this specific pressure level is favorable to optimal sputtering efficiency. Furthermore, it illustrates that as the applied voltage is increased, there is a corresponding increase in the intensity of the sputtered metals. This observation indicates that higher applied voltages enhance the sputtering process, which is attributed to the more energy available, resulting in more intense emission lines for both sputtering gas and sputtered atoms from the targets. However, in practice, operators of sputtering systems must carefully consider the optimal voltage settings by balancing the enhanced sputtering rate with the thin film quality and adherence to substrates [29].

Electron temperature (T_e) was determined using the Boltzmann-Plot method, considering variations in pressure and applied voltage based on emission lines from the Ar I species. The relationship between T_e and these emission lines relied on examining the linear correlation between the natural logarithm of the product $\text{Ln}(\lambda_{ji} I_{ji}/hcA_{ji} \cdot g_j)$ and the upper-level energy (E_{ji}). The high R^2 values in figures (5) and (6), indicating consistency and excellent line fitting, validate the precision of this approach in assessing T_e , which contributes to a comprehensive understanding of plasma conditions within the sputtering system under different experimental parameters.

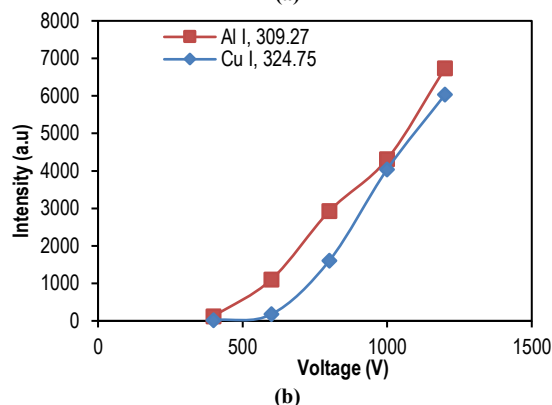
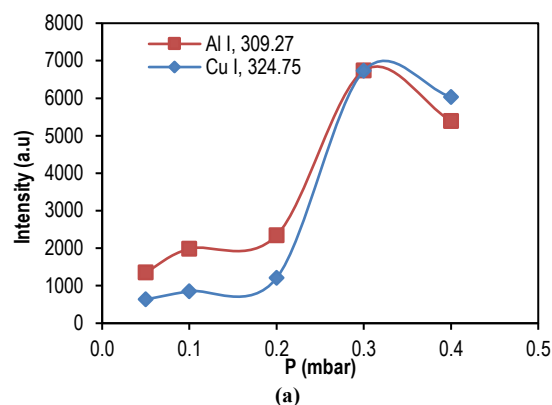
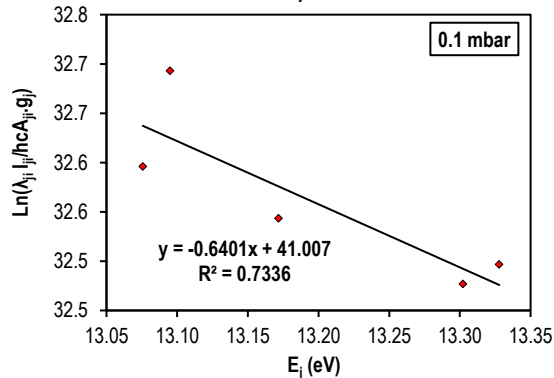
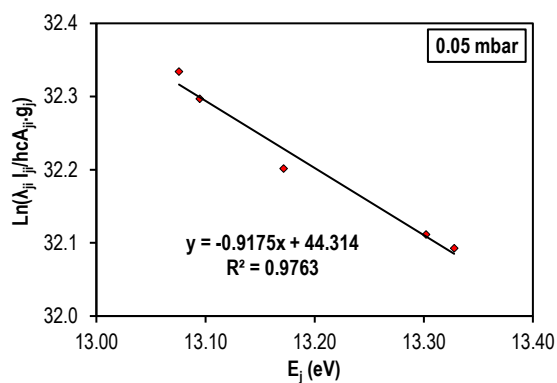


Fig. (4) Variation of Al I, 309.27 and Cu I, 324.75 intensity (a) with vacuum pressure at a constant applied voltage of 1200 V and (b) with applied voltage at a constant vacuum pressure of 0.3 mbar



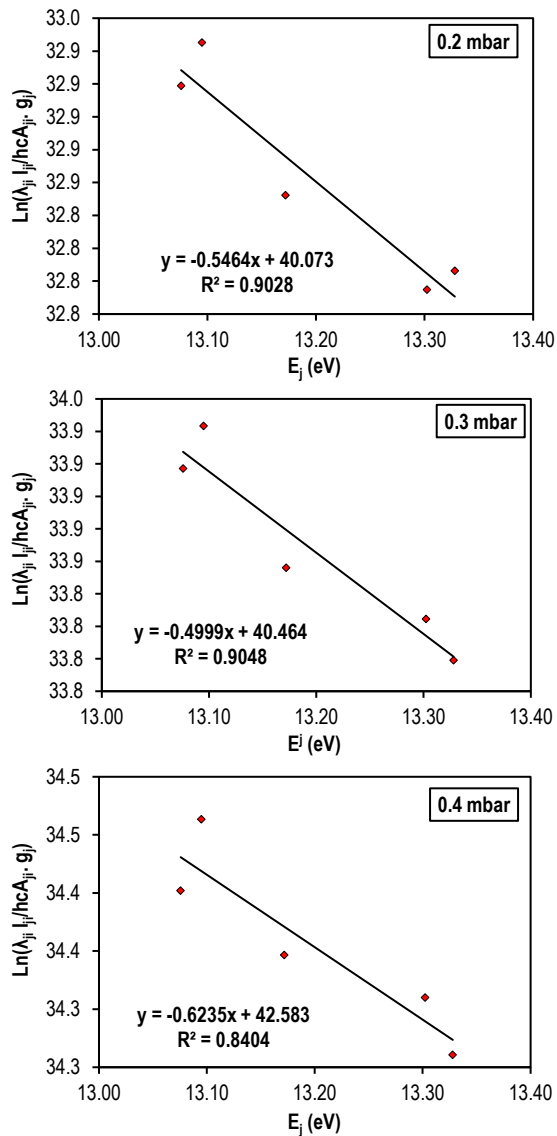


Fig. (5) Boltzmann-plot for Ar-I emission lines at different working pressures

Figure (7) presents the Lorentzian fitting applied to the Ar I (763.51 nm) emission lines observed under varying working pressures within an argon gas environment. As the gas pressure increases, the line becomes more broadening, peaking at 0.3 mbar and narrowing as the pressure is further raised to 0.4 mbar.

The increase in line broadening is mainly attributed to the influence of the increasing electron number density within the plasma (compared with other broadening processes, which can be neglected), correlated to the alterations in working pressure. Increasing pressure from 0.05 to 0.3 mbar causes growth in the electron number density due to the greater abundance of gas atoms available for ionization. The increase in electron density causes more frequent inelastic electron-neutral collision events [30,31]. However, as the working pressure is increased beyond 0.3 mbar, the available gas atoms for ionization become even more plentiful, leading to more electron-neutral collisions before electrons can

acquire sufficient energy for ionization. Instead, these electrons expend their energy in other types of collisions. This results in a decrease in the line broadening observed at 0.4 mbar gas pressure.

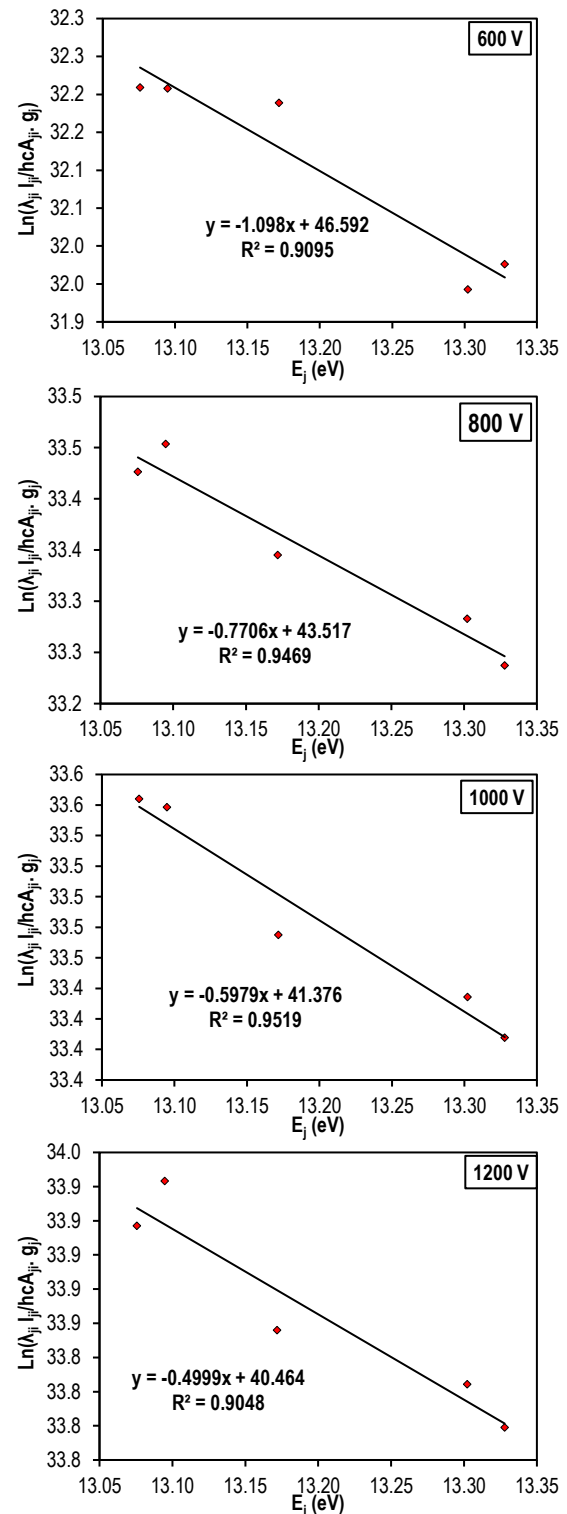


Fig. (6) Boltzmann-plot for Ar-I emission lines using different applied voltages at 0.3 mbar vacuum pressure

Figure (8) illustrates the Lorentzian fitting for the Ar I (763.51 nm) emission lines observed under varying applied voltages at a fixed working pressure of 0.3 mbar argon gas. The applied voltage range

from 600 to 1200V increases the emission lines' broadening. This broadening indicates a rise in electron number density within the plasma, attributed to the increased electron-neutral ionization collisions resulting from the increased energy gained by the free electrons due to the raised electric field.

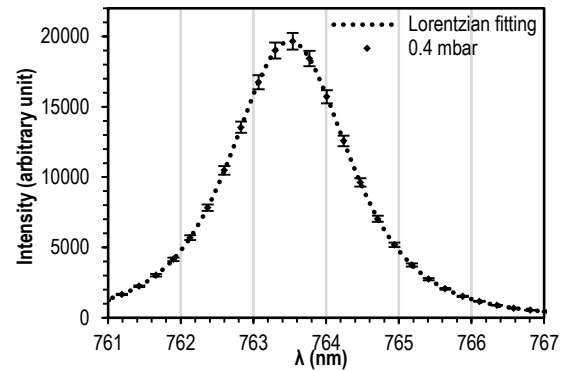
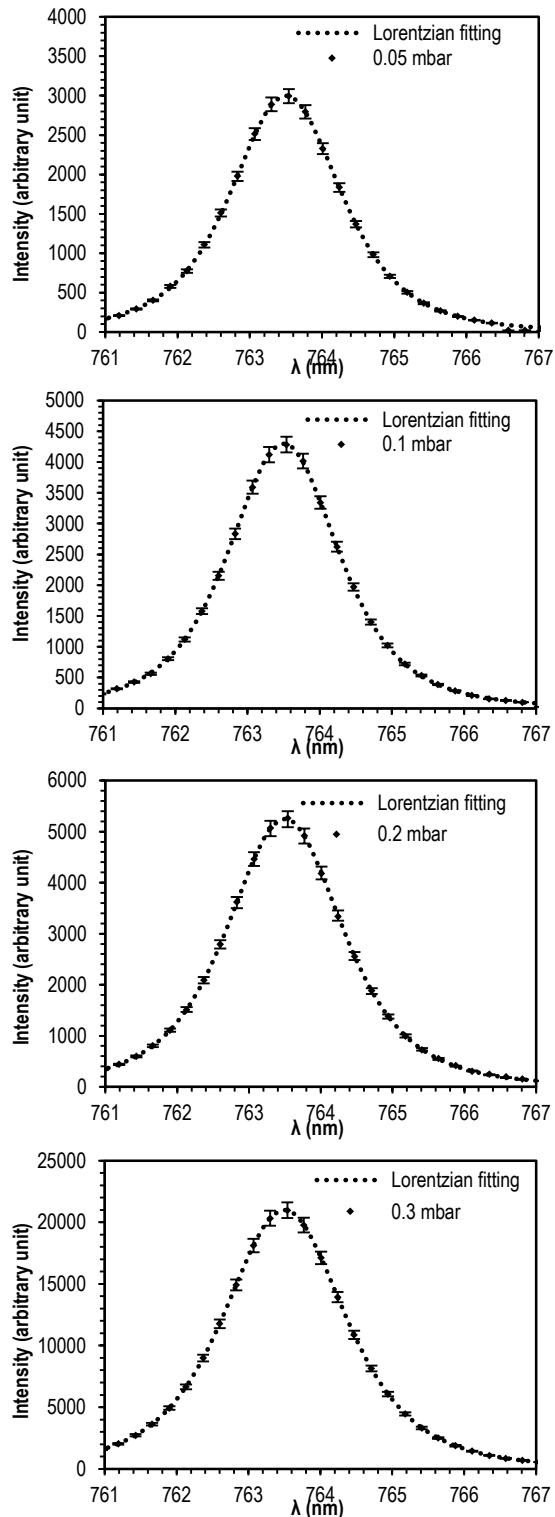


Fig. (7) Lorentzian fitting for the 763.51 nm Ar-I emission at different working pressures

The variation of T_e and n_e with the working pressure in the Argon environment observed within the sputtering system under different conditions, with varying vacuum pressures and applied voltages, were shown in figures (9) and (10). T_e and n_e exhibit an increase with rising pressure, reaching their peak values at a vacuum pressure of 0.3 mbar. Beyond this point, at 0.4 mbar pressure, T_e and n_e start to reduce. Higher pressures may increase collisions among gas particles, elevating the electron temperature [32]. This phenomenon explains why T_e increases with rising pressure, reaching its peak at an optimal pressure.

Further pressure increases beyond this point cause a reduction in electron temperature due to increased collisions and energy transfer from electrons to heavy atoms [33]. This optimal pressure for our setup configurations at 0.3 mbar pressure is linked to the efficiency of the sputtering process with the optimal plasma conditions. Both T_e and n_e decreased with increasing the working pressure to 0.4 mbar. Furthermore, higher voltages provide additional energy to the electrons, supporting the ionization process and increasing both T_e and n_e . These two fundamental characteristics of the plasma illustrate the behavior of the sputtering process trend and determine the optimal enhancing sputtering point [34].

Table (1) lists the plasma parameters for our co-sputtering configuration under different working conditions in argon at varying vacuum pressures and applied voltages. It includes electron temperature (T_e), electron number density (n_e), plasma frequency (f_p), Debye length (λ_D), and Debye number (N_D). The plasma parameters help characterize the behavior of the plasma within the system at varying conditions [35]. These parameters play a significant role in indicating sputtering efficiency. The variations in T_e and n_e are linked and related to other plasma parameters, reflecting the overall state of the plasma [36]. The highest values of T_e and n_e are observed at the optimal pressure of 0.3 mbar, while they tend to increase with increasing the applied voltage.

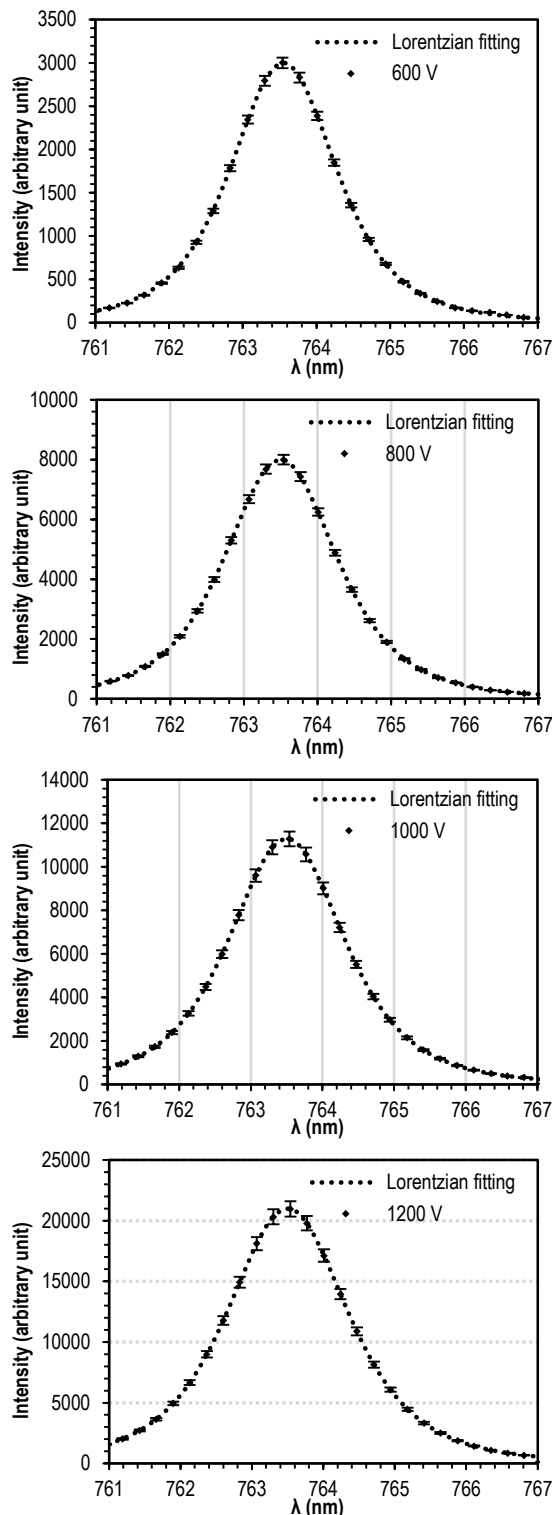


Fig. (8) Lorentzian fitting for the 763.51 nm Ar-I emission using different applied voltages at 0.3 mbar vacuum pressure

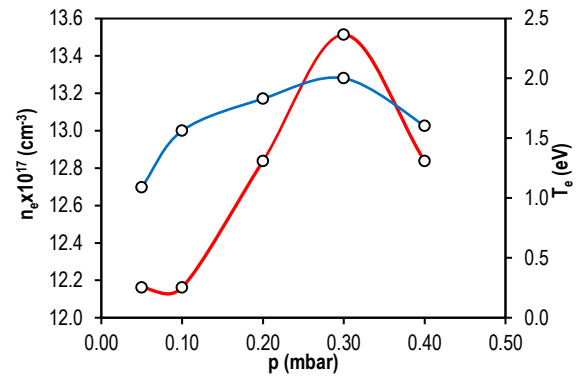


Fig. (9) Variation of electron number density and temperature with vacuum pressure

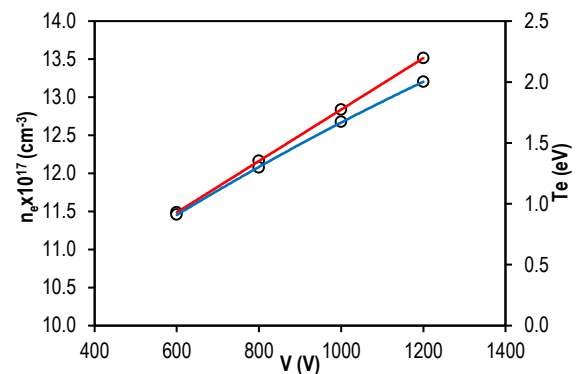


Fig. (10) Variation of electron number density and electron temperature with sputtering applied voltage at 0.3 mbar vacuum pressure

4. Conclusions

The spectroscopic diagnostics of Cu:Al plasma produced by dc magnetron discharge at different working conditions revealed that the optimal gas pressure for maximum line intensity was determined to be 0.3 mbar. In addition, a direct relationship between the applied voltage and emission line intensity was observed, with higher applied voltages resulting in increased line intensity corresponding to the sputtered species. The highest electron temperature and electron number density were recorded at 0.3 mbar, and both parameters increased with the applied voltage. These results provide precise quantitative data on how gas pressure and applied voltage influence the plasma parameters, aiding in the optimization of the sputtering process.

References

- [1] M.A. Khalaf, B.M. Ahmed and K.A. Aadim, "Spectroscopic analysis of CdO_{1-x}:Sn_x plasma produced by Nd:YAG laser", *Iraqi J. Sci.*, 61 (2020) 1665–1671.
- [2] V. Unnikrishnan et al., "Measurements of plasma temperature and electron density in laser-induced copper plasma by time-resolved spectroscopy of neutral atom and ion emissions", *Pramana - J. Phys.*, 74 (2010) 983–993.
- [3] R.J.E. Jaspers, "Plasma Spectroscopy", *Fusion Sci. Technol.*, 61 (2012) 384–393.

- [4] A. Ajith et al., "Comprehensive Analysis of Copper Plasma: A Laser-Induced Breakdown Spectroscopic Approach", *Photonics*, 10(2), (2023), 199.
- [5] A. Sergievskaya et al., "Magnetron sputter deposition of silver onto castor oil: The effect of plasma parameters on nanoparticle properties", *Colloids Surf. A Physicochem. Eng. Asp.*, 615 (2021) 126286.
- [6] J.-X. Zhang and Z.-Y. Zhao, "A comprehensive review on the preparation and applications of delafossite CuAlO₂ optoelectronic functional materials", *Mater. Sci. Semicond. Process.*, 167 (2023) 107819.
- [7] R.S. Mohammed, K.A. Aadim and K.A. Ahmed, "Synthesis of CuO/ZnO and MgO/ZnO Core/Shell Nanoparticles with Plasma Jets and Study of their Structural and Optical Properties", *Karbala Int. J. Mod. Sci.*, 8 (2022) 88–97.
- [8] S.Z. Wu, "Dependence of plasma characteristics on dc magnetron sputter parameters", *J. Appl. Phys.*, 98 (2005).
- [9] A. Ojeda-G-P, M. Döbeli and T. Lippert, "Influence of Plume Properties on Thin Film Composition in Pulsed Laser Deposition", *Adv. Mater. Interfaces*, 5 (2018) 1–16.
- [10] K.A. Aadim, "Detection of laser-produced tin plasma emission lines in atmospheric environment by optical emission spectroscopy technique", *Phot. Sens.*, 7 (2017) 289–293.
- [11] E. Ajenifuja, A.P.I. Popoola and O.M. Popoola, "Thickness dependent chemical and microstructural properties of DC reactive magnetron sputtered titanium nitride thin films on low carbon steel cross-section", *J. Mater. Res. Technol.*, 8 (2019) 377–384.
- [12] J.W. Low et al., "Spectroscopic studies of magnetron sputtering plasma discharge in Cu/O₂/Ar mixture for copper oxide thin film fabrication", *J. Teknol.*, 73 (2015) 11–15.
- [13] S.N. Mazhir et al., "Measurement of plasma electron temperature and density by using different applied voltages and working pressures in a magnetron sputtering system", *Int. J. Eng. Technol.*, 7 (2018) 1177.
- [14] S. Singh, S. Karthick and I.A. Palani, "Design and development of Cu–Al–Ni shape memory alloy coated optical fiber sensor for temperature sensing applications", *Vacuum*, 191 (2021) 110369.
- [15] S.A. Gad et al., "Impact of chromium doping on structural, optical, magnetic and electrical properties of nano-copper ferrite", *J. Ovonic Res.*, 16 (2020) 293–308.
- [16] S.K. Mustafa, R.K. Jamal and K.A. Aadim, "Studying the Effect of Annealing on Optical and Structure Properties of ZnO Nanostructure Prepared by Laser Induced Plasma", *Iraqi J. Sci.*, (2019) 2168–2176.
- [17] B. Adamiak et al., "Preparation of multicomponent thin films by magnetron co-sputtering method: The Cu-Ti case study", *Vacuum*, 161 (2019) 419–428.
- [18] K.A. Aadim, "Optical emission spectroscopic analysis of plasma parameters in tin–copper alloy co-sputtering system", *Opt. Quantum Electron.*, 48 (2016) 545.
- [19] S.T. Hsieh et al., "The Correlation of Plasma Characteristics to the Deposition Rate of Plasma Polymerized Methyl Methacrylate Thin Films in an Inductively Coupled Plasma System", *Coatings*, 12 (2022).
- [20] K.A. Aadim, A.Z. Mohammad and M.A. Abduljabbar, "Influence of laser energy on syntheses of CdO/Nps in liquid environment", *IOP Conf. Ser. Mater. Sci. Eng.*, 454 (2018).
- [21] NIST Atomic Spectra Database (Version 511), online available: <https://www.nist.gov/pml/atomic-spectra-database>.
- [22] A.F. Ahmed, K.A. Aadim and A.A. Yousef, "Spectroscopic study of AL nitrogen plasma produced by DC glow discharge", *Iraqi J. Sci.*, 59 (2018) 494–501.
- [23] A. Ahmed et al., "Blushers component analysis for unbranded cosmetic brands: Elements' concentration levels and its effect on human body", *J. Adv. Res. Dyn. Control Syst.*, 11 (2019) 412–419.
- [24] J.T. Gudmundsson, "Physics and technology of magnetron sputtering discharges", *Plasma Sources Sci. Technol.*, 29 (2020) 113001.
- [25] R.M.S. Al-Haddad, I.M. Al-Essa and S.A.-D.M. Al-Dowaib, "Optical properties of TiO₂ thin films prepared by reactive d.c magnetron sputtering", *Iraqi J. Phys.*, 10 (2012) 69–75.
- [26] M.M. Abdelrahman, "Study of Plasma and Ion Beam Sputtering Processes", *J. Phys. Sci. Appl.*, 5 (2015).
- [27] N.K. Abdaalameer, S.N. Mazhir and K.A. Aadim, "Diagnostics of zinc selenite plasma produced by FHG of a Q-switched Nd:YAG laser", *Chalcogen. Lett.*, 18 (2021) 405–411.
- [28] R. Wang et al., "Influence of Target Current on Structure and Performance of Cu Films Deposited by Oscillating Pulse Magnetron Sputtering", *Coatings*, 12 (2022) 394.
- [29] R. Tang et al., "Controlled Sputtering Pressure on High-Quality Sb₂Se₃ Thin Film for Substrate Configured Solar Cells", *Nanomaterials*, 10 (2020) 574.
- [30] K.A. Aadim, "Spectroscopic study for plasma parameters in co-sputtering system", *Iraqi J. Phys.*, 14 (2024) 122–8.
- [31] T.M. Saleh and F.J. Kadhim, "Langmuir Characteristics of Glow Discharge Plasma in DC Reactive Magnetron Sputtering System", *Iraqi J. Mater.*, 3(1) (2024) 25–32.
- [32] S.N. Rashid, K.A. Aadim and A.S. Jasim, "Silver

- Nanoparticles Synthesized By Nd:YAG Laser Ablation Technique: Characterization and Antibacterial Activity", *Karbala Int. J. Mod. Sci.*, 8 (2022) 71–82.
- [33] J. Held, M. George and A. von Keudell, "Spoke-resolved electron density, temperature and potential in direct current magnetron sputtering and HiPIMS discharges", *Plasma Sources Sci. Technol.*, 31 (2022) 085013.
- [34] R.K. Jamal et al., "Hydrogen gas sensors based on electrostatically spray deposited nickel oxide thin film structures", *Phot. Sens.*, 5 (2015) 235–240.
- [35] P. Riccardi, "Electron Spectroscopy of Charge Exchange Effects in Low Energy Ion Scattering at Surfaces: Case Studies of Heavy Ions at Al Surface", *Surfaces*, 6 (2023) 64–82.
- [36] H.J. Imran et al., "Preparation Methods and Classification Study of Nanomaterial: A Review", *J. Phys. Conf. Ser.* 1818 (2021).

Table (1) Plasma parameters for the co-sputtering DC discharge in Ar at different working pressures and applied voltages

P (mbar)	V (V)	T _e (eV)	FWHM (nm)	n _e × 10 ¹⁷ (cm ⁻³)	f _p × 10 ¹² (Hz)	λ _D × 10 ⁻⁶ (cm)	N _D
0.05	1200	1.090	1.800	12.162	9.903	7.034	1773
0.10		1.562	1.800	12.162	9.903	8.421	3042
0.20		1.830	1.900	12.838	10.175	8.871	3755
0.30		2.001	2.000	13.514	10.439	9.040	4182
0.40		1.604	1.900	12.838	10.175	8.305	3080
0.3	600	0.911	1.700	11.486	9.624	6.616	1393
	800	1.298	1.800	12.162	9.903	7.675	2303
	1000	1.673	1.900	12.838	10.175	8.481	3280
	1200	2.001	2.000	13.514	10.439	9.040	4182